Journal of
Synchrotron Radiation

ISSN 0909-0495

Received 14 September 2007
Accepted 27 September 2007

Time–space transformation of femtosecond free-electron laser pulses by periodical multilayers

Dmitriy Ksenzov, Souren Grigorian* and Ullrich Pietsch

University of Siegen, Germany. E-mail: grigorian@physik.uni-siegen.de

A scattering scheme to probe the time evolution of femtosecond pulses of a soft X-ray free-electron laser (FEL) in a multilayer structure is presented. The response of periodic multilayers (MLs) with low and high absorption and various numbers of bi-layers to a pulse train of Gaussian-shaped sub-pulses is calculated. During the passage of the incident pulse the interaction length increases and the scattering profile changes as a function of the spatial position of the pulse within the sample. Owing to stretching of the reflected pulse compared with the incident pulse, the time-dependent scattering evolution in the ML can be visualized along a spatial coordinate of a position-sensitive detector. Using a scattering geometry where the mean energy of the incident pulse train is slightly detuned from the energy of maximum reflectivity at the first-order peak, the response of the ML shows an oscillator behaviour along this spatial coordinate at the detector. For a FEL wavelength of 6.4 nm this effect is promising for MLs with low absorption, such as La/C for example. On the other hand, the oscillations will not be present for MLs with high absorption. Therefore a low-absorbing ML is a sensitive tool for studying the possible change of sample absorption caused by femtosecond-pulse interaction with matter.

Keywords: multilayers; femtosecond pulses; free-electron laser.

1. Introduction

Motivated by current projects to build X-ray free-electron lasers (XFEL) in several places in the world, there is a growing interest in the fundamental physics of X-ray diffraction from crystals on femtosecond (fs) time scales. In the case of pulse generation in the self-amplified spontaneous-emission (SASE) regime the XFEL will produce a pulse train of duration a few hundred fs which is almost fully coherent in the transverse direction. The pulse train consists of a substructure of single spikes with sub-fs duration and slightly different energy (DESY Report, 2006*a*). High-resolution diffraction experiments require the selection of a certain mode from an XFEL pulse using the X-ray diffraction profile by a single (monochromator) crystal. This appears to be difficult because each sub-pulse of a pulse train additionally becomes transformed by the crystal. The response of a perfect crystal to fs-XFEL radiation has been studied by Shastri *et al.* (2001) and Graeff (2004). Neglecting the time- and/or intensity-dependence of crystal absorption, these calculations show that each individual sub-pulse becomes stretched in time owing to the duration of radiation propagation through the crystal. The general properties of crystal diffraction by fs X-ray pulses have been derived from time-dependent Takagi–Taupin equations (Chukovskii & Förster, 1995; Wark & He, 1994). By considering X-ray absorption from unperturbed crystals, time-dependent features were found in the diffraction curve such as the evolution of Pendellösung fringes. The possible influence of high intensity was studied on 'laser-heated' crystals by Wark & Lee (1999). Unfortunately, these theoretical studies cannot be verified until installation of an XFEL is completed. However, FLASH (a free-electron laser in Hamburg) at DESY is in operation in the soft X-ray regime (Ackermann *et al.*, 2007). First experiments have been performed which verify the expected time structure (Ayvazyan *et al.*, 2002) and the excellent coherent properties (see, for example, Chapman *et al.*, 2006). In addition, the crystal becomes destroyed by the highly intense beam (Stojanovic *et al.*, 2006). Extensive cooling strategies are proposed to avoid destruction in order to use crystals as monochromators (DESY Report, 2006*a*), neglecting phenomena which may modify absorption and heat dissipation. Hau-Riege *et al.* (2006) have shown recently that on a fs time scale the reflectivity of a Si/C multilayer excited by FLASH pulses of wavelength 32 nm can still be described by Parratt's formalism.

An X-ray diffraction experiment where the single crystals are replaced by a multilayer mirror can already be performed using VUV FEL radiation wavelengths of a few nanometres. FLASH, for example, will generate FEL pulses with 20–50 fs pulse length and a sub-pulse duration of about 2–3 fs at an average wavelength of 6.4 nm (DESY Report, 2006*b*). Moreover, the performance of specially designed multilayers

as beam chopper systems of hard XFEL pulses has been reported by Krenza & Meyer-ter-Vehn (2005). The response of a multilayer (ML) to hard X-ray XFEL pulses has been simulated by Tatchyn & Bionta (2001). Similar to crystals (Shastri *et al.*, 2001; Graeff, 2004), there is a certain time delay of the reflected pulse relative to the incident pulse. Hence the delay time depends on absorption; it subsequently determines the effective penetration depth of the FEL pulse into the material. For a ML the effective penetration depth corresponds to a certain number of layers probed by the incident radiation. The shape of the reflection curve will change during the propagation of the pulse through the ML structure owing to the interaction of the beam with an increasing number of bi-layers. Study of the time-dependent response of the ML to the X-ray pulse can provide insight into the process of interaction of highly intense FEL radiation with matter. Using an appropriate geometrical set-up of the experiment the time structure of the reflected pulse can be transformed into a spatial coordinate of a position-sensitive detector (Lindenberg *et al.*, 2005).

The current paper is organized as follows. First we calculate the general ML response to Gaussian-shaped fs pulses for low- and high-absorbing materials depending on the number of ML periods. We show the evolution of the reflected signals as a function of penetration depth into the ML. The response of the ML will be analyzed for exact Bragg or slightly detuned conditions. Finally the possibility of visualizing pulsed substructure from the integrated signal of the spatial detector side will be discussed.

2. Basic calculations

The calculations were performed for a wavelength of 6.4 nm as provided by FLASH. This wavelength requires a scattering object with lattice parameters in the range of a few nanometres. Such an object can be a ML structure prepared by repetitions of thin layers of two different materials. In the case of a FEL the incident radiation is a pulse train composed of ultrashort pulses of a few fs duration. The simulation of the ML response to such a pulse requires a certain approximation of its shape.

Usually ultrashort pulses are described in time or frequency space by either δ or Gaussian functions. The use of δ functions leads to simple analytical solutions, and the frequency range of the incident pulses is not limited (Shastri *et al.*, 2001). For VUV radiation the assumption of a Gaussian shape for an incident pulse is a more realistic model (Hau-Riege *et al.*, 2007; Ayvazyan *et al.*, 2006) which also allows Fourier transformation to be performed in a simple way.

An experiment with fs pulses has to be performed at fixed scattering geometry. Therefore the first step of the simulation consists of calculating the complex amplitude of reflection as a function of frequency for a fixed angle of incidence with respect to the ML normal and using symmetric scattering geometry. We consider a stack of N bi-layers consisting of two layers of different thicknesses. The complex dielectric constants of each sub-layer are expressed in terms of complex X-ray refraction coefficients considering the energy-dependent X-ray absorption. The reflectivity of the periodical ML is calculated using Parratt's recursive method (Parratt, 1954; Kohn, 1995). Using a linear-optics reflection theory (Eilbeck, 1972), the calculation of the ML response to an incident pulse train is performed using the following steps. First, each incident pulse is described by a single Gaussian and subsequently the pulse train by a combination of several Gaussian functions of the same width. Next, the time structure of an incident pulse train is spectrally decomposed by use of Fourier transformation. Finally, within the spectral range of emission, each Fourier component of the incident pulse amplitude is multiplied by the complex reflection amplitude of the ML followed by inverse Fourier transformation in order to find the time response of the reflected pulses.

Table 1
Correction to refraction index ($n = 1 - \delta + i\beta$) for different materials at 193.75 eV with increasing absorption coefficient.

Element/compound	δ	β
C	0.0079	0.00063
La	0.0138	0.00097
Sc	0.0065	0.00232
Nb	0.0084	0.00252
Mo	0.0113	0.00278
Ru	0.0167	0.00378
RhRu	0.0170	0.00393
Y	0.0016	0.00541
V	0.0159	0.00579
Cr	0.0197	0.00761
Si	0.0077	0.00838
B_4C	0.0028	0.00855
Al_2O_3	0.0169	0.00892
B	0.0010	0.00996
Fe	0.0222	0.01165
CrB_2	0.0148	0.01436
Ni	0.0237	0.01694

3. Reflectivity of periodical multilayers

Typical multilayer mirrors for soft X-rays consist of a periodic stacking of high-refracting (Mo, Ni, Cr, Ru, Fe, V) and low-refracting (C, Si, B_4C) materials. By using various combinations of these materials the optical properties of the respective optical element can be tuned in terms of transmission, absorption and reflection. The shape and the total scattering power at fundamental Bragg reflections are influenced by the number of stacked bi-layers (for example, Born & Wolf, 1999; Vinogradov *et al.*, 1989).

For a FEL wavelength of 6.4 nm the ML reflectivity is generally low for a few reasons. First, the optical constants for this wavelength are very similar (see Table 1) and a combination of two materials does not provide a large scattering contrast. Second, the absorption coefficient is large for most of the materials. Both peculiarities limit the effective penetration depth into the ML. Third, in order to tune the first-order Bragg peak of the ML to a scattering angle 2Θ, the bi-layer period must be smaller than 10 nm. Under these circumstances an interface roughness of a few atomic layers can significantly reduce the reflectivity (Takenaka *et al.*, 2005).

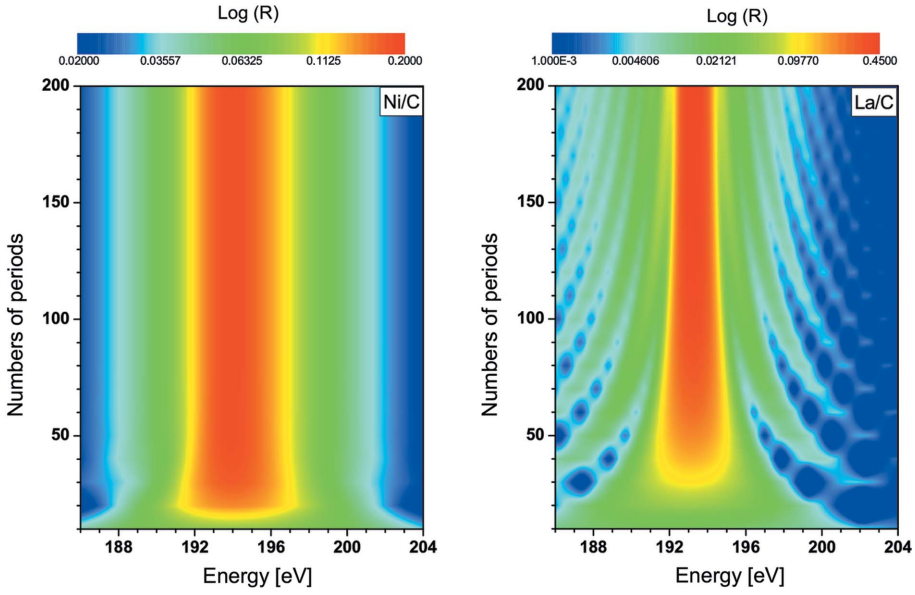

Figure 1
Calculated reflectivity of MLs as a function of energy and number of bi-layers. High-absorbing Ni/C (left) and low-absorbing La/C (right).

In the follow we consider the combination of La and C, and Ni and C, as materials with high scattering contrast. However, La and Ni have different absorption properties in this energy range. For $\lambda = 6.4$ nm (193.75 eV) the bi-layer spacing has to be $d = 4.62$ nm for these MLs so that the first-order diffraction maximum is appearing at $2\Theta = 90^\circ$. The variations in the reflectivity spectra for both MLs are shown in Fig. 1 as a function of the number of bi-layers. Calculations were performed by using Parratt's recurrent formalism considering a thickness ratio of 0.5 and continuous strictly parallel VUV radiation. Owing to the high absorption of Ni layers the reflectivity curve of the Ni/C sample saturates after penetration of about 40 bi-layers at a maximum reflectivity of about 18% and does not show any internal structure. The response of the low-absorbing La/C ML is shown in Fig. 1 (right). Here the intensity increases with the number of bi-layers, reaching a maximum of about 40% for a ML with more than 120 bi-layers. In addition, thickness oscillations decrease with increasing number of bi-layers. The energy width of the central maximum is about 6 eV for Ni/C and about 1.5 eV for La/C MLs with large numbers of bi-layers.

4. Numerical simulation of fs-pulse responses from multilayers

FLASH emits a pulse train of duration 20–50 fs consisting of sub-pulses of about 2–3 fs in length. For this source the shape of such pulses has been experimentally verified for a wavelength of 33 nm (Ayvzyan *et al.*, 2006) and recently for 13 nm (Ackermann *et al.*, 2007). A similar pulse structure is proposed for a wavelength of 6.4 nm.

First let us consider the ML response to a single Gaussian pulse of duration 2 fs (one sub-pulse of a VUV FEL pulse train) for La/C and Ni/C MLs as a function of the number of bi-layers N at a fixed incidence angle of $\theta = 45^\circ$. The low- and high-absorbing ML responses are shown in Fig. 2. As in Fig. 1, essential differences in the responses of these MLs may be seen (Figs. 2*b* and 2*c*). When the initial pulse strikes the ML with different numbers of bi-layers, only the first $N \simeq 40$ bi-layers strongly contribute to the scattering process for the high-absorbing Ni/C ML. Owing to almost complete absorption of the pulse within the first few layers, the duration of the reflected pulse is approximately the same as that of the initial one (Figs. 2*a* and 2*b*). In contrast, the reflected pulse is expanded to 2 fs compared with the initial pulse for the low-absorbing La/C ML. The pulse expansion increases with the number of bi-layers N, reaching certain saturation at $N = 120$ for the La/C ML. A maximum reflectivity of about 28% is reached at $N \simeq 100$ (Fig. 2*c*). In all three cases shown in Fig. 2 the energy of the incident pulses coincides with the maximum of the first ML Bragg peak of the reflection curve at a given angle of incidence. Changing the scattering angle or/and the energy of the incident pulse, E_i, differs from the energy of the central maximum of reflectivity, E_{max}, by $\Delta E = E_i - E_{max}$. Fig. 2(*d*) shows the time-dependent response of the La/C multilayer for $\Delta E \simeq 3$ eV. Now the reflectivity of the La/C ML is reduced (by a few percent) but reveals a certain variation of intensity as a function of N, which is not visible for Ni/C. This asymmetry increases for increasing ΔE (not shown). Moreover, for the longer pulses (4 fs and more) one finds an oscillatory behaviour of reflection intensity as a function of N (see later). These features can be explained by the fine structure of the scattering curves as schematically shown in Fig. 3. By changing E_i relative to E_{max} one can excite different spectra, from continuous to oscillating features as a functionn of N. The ML response to a pulse is an integration of the scattering curve within a certain energy window. If $\Delta E \simeq 0$, *i.e.* $E_i \simeq 193.75$ eV as in the present example (Fig. 3*c*), the scattering phases between different interfaces is always constructive and the response is a smooth function for increasing N (see Fig. 3*a*). If the energy shift ΔE is larger than the energy width of the total reflection curve (Fig. 3*d*), the phase shift might be constructive at certain N but destructive for another $N + \Delta N$. This oscillatory behaviour of scattering as a function of N is shown in Fig. 3(*b*). Such an effect can be used to identify the energy offset of the incident pulse with respect to the central reflection maximum fixed by a certain geometric set-up.

For simulation of an incident pulse train, every pulse is composed of several sub-pulses of duration 2–3 fs. Considering the SASE principle, each of these sub-pulses (spikes) is spatially separated from each other and described by Gaussian functions with varying amplitude. Additionally the spikes differ in energy within a certain energy window of about 2 eV

as expected for FEL radiation. Using this approach one can change the shape of any incident pulse train by changing the spike parameters, *e.g.* the amplitude, frequency, location and duration of the Gaussian-shaped sub-pulses, as shown in Fig. 4(*a*). The results of numerical calculation for both MLs are illustrated in Figs. 4(*b*)–4(*d*). Since the mean energy of the incident pulse train coincides with the energy of maximum reflectivity of the ML the diffraction curves for both MLs show

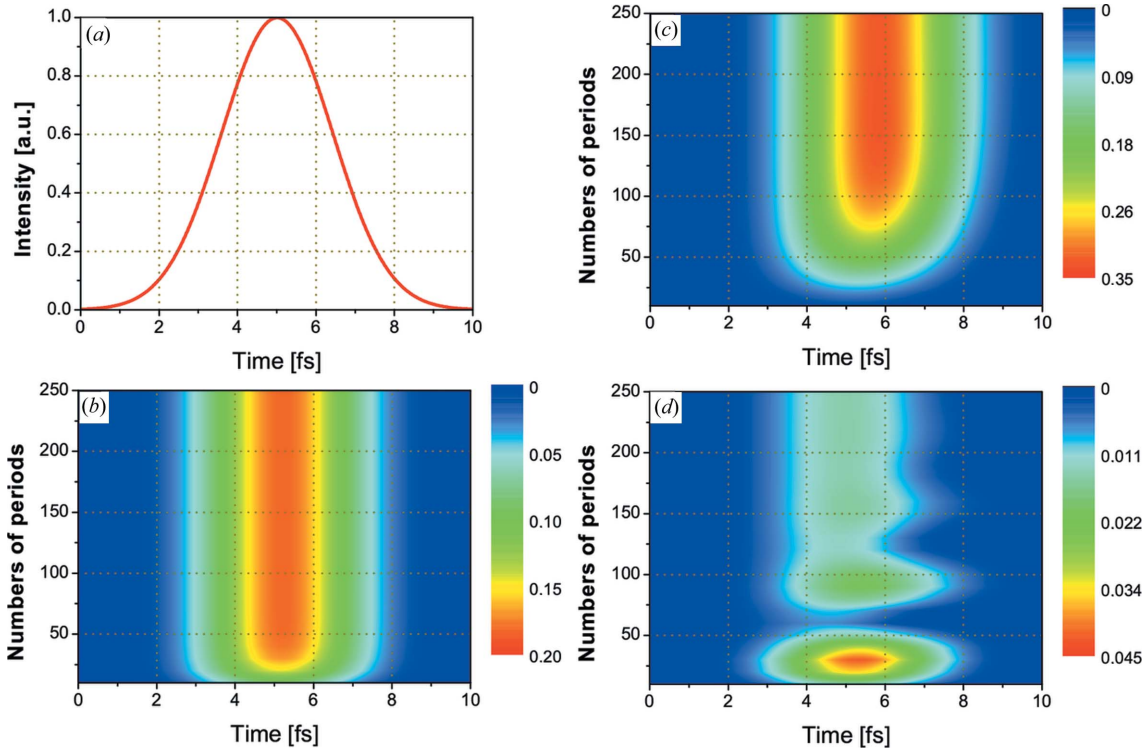

Figure 2
Incident single pulse (*a*) and time responses from various periodical Ni/C (*b*) and La/C (*c*, *d*) MLs. The duration of the incident single Gaussian pulse is 2 fs and the energies are 193.75 eV (*b*, *c*) and 191 eV (*d*).

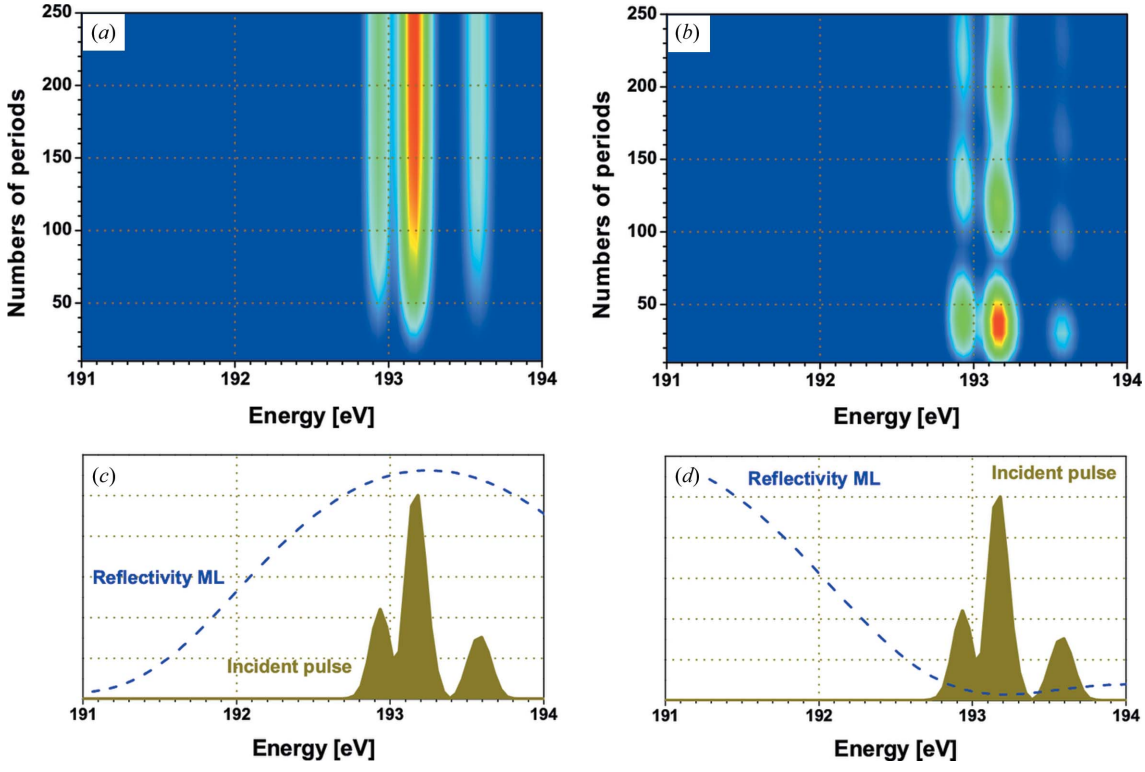

Figure 3
Transition of the energy spectra from continuous to oscillatory depending on energy shift ΔE (*a*) without energy shift, $\Delta E = 0$, and (*b*) with energy shift $\Delta E \simeq 3$ eV. The energy relation between the incident pulse train and the reflection curve is shown in (*c*) and (*d*).

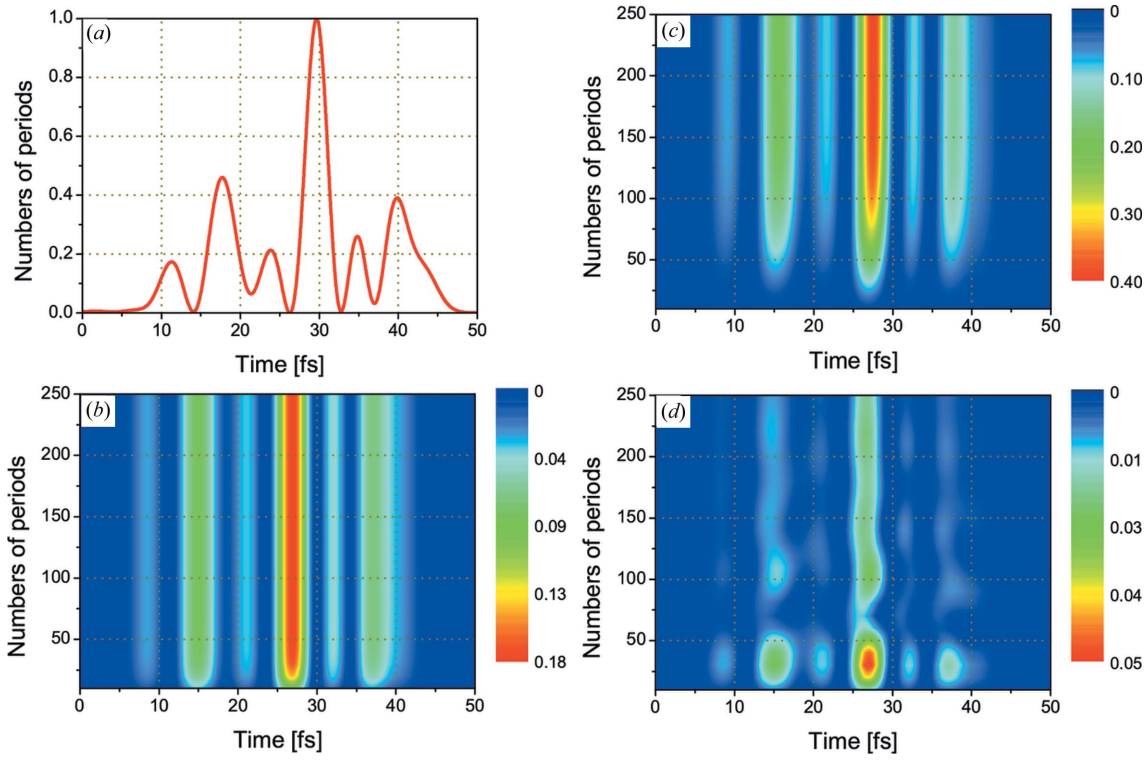

Figure 4
Incident multiple pulse (*a*) and responses from periodical Ni/C (*b*) and La/C (*c*, *d*) MLs with different numbers of bi-layers. The incident pulses describe the combination of the single-Gaussian function with different parameters: frequency, amplitudes, locations and durations in the time range (*a*). The responses from the La/C ML with an energy shift of the incident pulse train of 3 eV (*d*).

a mirror-like behaviour of the incident pulse structure where each sub-pulse is expanded (see Figs. 2*b* and 2*c*). Such behaviour was observed for the Ni/C and La/C MLs shown in Figs. 4(*b*) and 4(*c*), respectively. The response of the La/C ML changes if the mean energy of the pulse train differs by ΔE from the energy of the reflection maximum. Fig. 4(*d*) shows the situation for the energy shift ΔE = 3 eV. In contrast to Fig. 4(*c*), an oscillatory behaviour of the response functions of Fig. 4(*d*) is found in the time and the energy domain. The corresponding pictures in the energy domain are shown in Figs. 3(*a*) and 3(*b*). For different sub-pulses one finds a different response. One should mention that such a redistribution of the response function can be achieved either by detuning the energy or the incident angle or by changing the structural parameters of the ML. Therefore a careful structural analysis of the ML is mandatory before the FEL experiment.

5. Possible experimental realisation of space–time transformation

A reasonable scenario of such a scattering experiment consists of the projection of the time-dependent response of the ML to the incident FEL pulse into a spatial coordinate which can be measured by a position-sensitive detector. This strike-camera-like concept has already been used for observation of fs pulses at the Sub-Picosecond Pulse Source of the Stanford Linear Accelerator Center (Lindenberg *et al.*, 2005), and the use of a novel CCD detector for visualization of diffractive imaging has been reported by Chapman *et al.* (2006).

Owing to the pulse structure of the incident X-rays the whole ML response is not detected at the same time. As the incident pulse reaches the first bi-layer interface it provides a strong scattering signal towards the detector. On its passage through the ML the pulse interacts with more and more bi-layers which modifies the intensity and the shape of the scattering signal in a fashion shown in Figs. 2–4. In this sense the vertical coordinates of Figs. 2 and 4 (the number of bi-layers) can be transformed into a spatial coordinate seen by the detector.

Owing to the fs time-structure of irradiation, all sub-pulses will coincide on the detector. However, using a scattering geometry where the mean energy of the incident pulse is slightly detuned from the maximum of the reflectivity of the first-order Bragg reflection, the oscillatory behaviour can be maintained even after an overlapping of all the sub-pulses. This is shown in Fig. 5 for the case of low-absorbing (La/C) and high-absorbing (Ni/C) ML materials. The spatial coordinate x reflects the evolution of the scattered signal as a function of the increasing number of interfaces N of the ML. The oscillatory behaviour is preserved for the low-absorbing ML and varies as a function of the detuning energy. In contrast, there is no such dependence in the high-absorption case. This is because the absorption length for radiation at a wavelength of 6.4 nm is about 1.7 µm for La/C but only 0.1 µm for Ni/C. At the same time the geometric length of a 2 fs pulse is 0.6 µm corresponding to N = 134 periods of the ML.

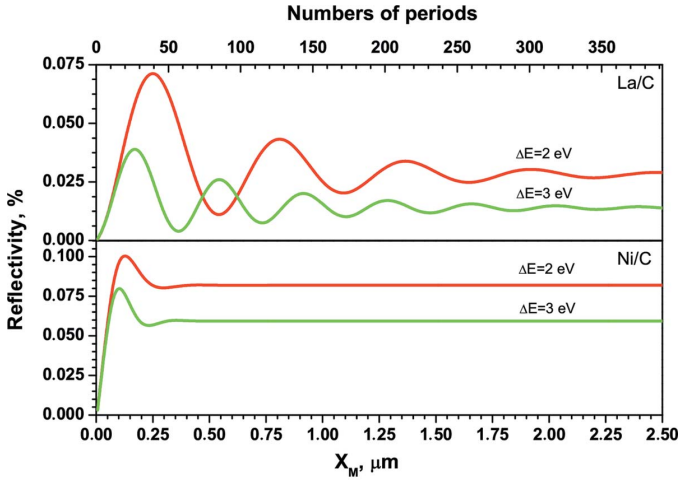

Figure 5
Spatial variation of the reflected intensity for La/C and Ni/C MLs as a function of the detuning energy $E_{max} - \Delta E$. The energy of the central maximum reflection E_{max} is 193.75 eV.

Considering a ML with $N = 400$, for example, the interaction length within the ML and subsequently the length of the diffraction spot in the detector plane, x_M, is 2.5 μm. This length can be stretched in space by use of a ML where the surface has a sliced angle α with respect to the multilayer normal. If the incident pulse hits the ML interfaces at a scattering angle $\Theta \simeq 45^\circ$, a grazing incident angle with respect to the ML surface of $\Theta - \alpha$ will enlarge the effective size of the reflected beam by $1/\sin(\Theta - \alpha)$. An additional enlargement of x_M can be achieved by oblique setting of the detector with respect to the reflected beam by an angle β of the detector normal with respect to the reflected beam. For a La/C ML and using $\Theta - \alpha \simeq 2^\circ$ and $\beta \simeq 5^\circ$, one can reach a stretching factor larger than 300 for the detector coordinate x_M which corresponds to 137 pixels of a CCD with pixel size 6 μm (Gerth *et al.*, 2001). This might be sufficient to detect the appearance or disappearance of the oscillations shown in Fig. 5.

To exploit the effect of La/C film the number of ML periods should be very large ($N > 1000$). Sliced multilayer gratings (SMGs) are well suited to this task and give rise to surface gratings in addition to the strong Bragg reflection. Whereas the Bragg reflection probes the bulk scattering of the ML, the grating peaks are created by scattering at the surface relief. The latter ones can be used as an independent probe of the energy of the sub-pulses without interaction with the bulk of the ML.

The complete theory of reflection and transmission from sliced ML gratings was derived by Kogelnick (1969) in terms of coupled wave equations and further developed by Levashov & Vinogradov (1993) and Fechtchenko *et al.* (2002). For these structures the energy width of the diffraction pattern increases with increasing sliced angle α and using grazing-incidence geometry. The evolution of diffraction efficiency as a function of α and Θ (both parameters are coupling for the resonance case) for La/C with $d = 4.7$ nm and a thickness ratio of 0.5 is shown in Fig. 6. As shown on the right-hand side of

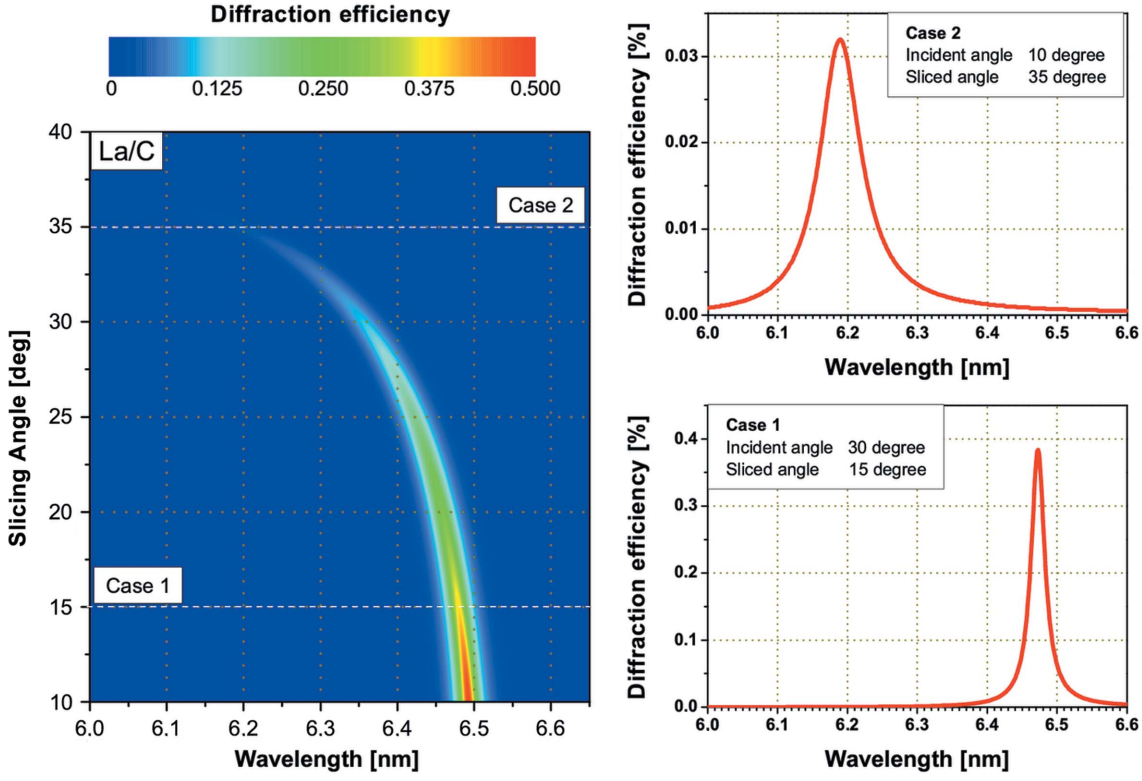

Figure 6
Calculated diffraction efficiency as a function of wavelength, incident angle and slicing angle. Cases 1 and 2 correspond to relatively small and large slicing angle and reveal different broadening of the diffraction efficiency curves.

Fig. 6, the FWHM of the diffraction maximum increases by a factor $[\sin(\theta + \alpha)/\sin(\theta - \alpha)]^{1/2}$, increasing the sliced angle α, and the energy position of the scattering maximum is shifted to a lower wavelength accompanied by a reduction in the total scattering power, known from X-ray dynamical theory. For comparison, shown at $\alpha = 0$ the FWHM is increased by factors of 1.32 and 2.38 for cases 1 and 2, respectively, in Fig. 6.

For $d = 4.7$ nm and $\alpha = 35^\circ$ (and grazing angle = 10°) (case 2 in Fig. 6) the effective grating spacing $D = d/\sin\alpha = 8.2$ nm, which gives the first-order grating peak at $\Theta_m = 10^\circ$. However, owing to the finite length of the incident sub-pulse (duration 50 fs), the number of illuminated grating periods is large (here about 1600) resulting in a narrow grating peak. Therefore measurement of the angular position and angular width of the grating peak is an independent and precise probe of the energy and the energy spread of the incident pulse.

6. Conclusions

We have analyzed the interaction of VUV FEL pulses with a multilayer. Owing to the finite length of a pulse the evolution of the multilayer response can be studied as a function of the penetration depth of the incident pulse into the ML. For this purpose MLs with low absorption and high reflectivity, such as La/C MLs, are promising candidates. The behaviour of the interaction of the incident pulse with the ML can be varied by setting the angle of incidence with respect to the ML surface at certain values. The evolution of ML reflectivity as a function of the number of interfaces becomes visible if the mean energy of the incident pulse differs by a small amount ΔE from the energy of the maximum reflectivity at the first-order Bragg peak. Using the ML as a monochromator for the following experiment, such a detuned scattering geometry can be an option for tailoring the reflection intensity. The time–space transformation can be improved using sliced MLs and an asymmetric scattering geometry. Here the length of the reflected pulse at the detector is a direct measure of the absorption length within the sample. Any effect of a modified interaction, owing to non-linear absorption or electronic excitation, which would result in a reduction of the effective absorption length, becomes directly measurable by such a scattering experiment.

It is important to note that all effects that are linked with the high intensity of FEL radiation are not considered in this work. Various excitation phenomena can play an important role in the process of the interaction of FEL radiation with materials and may eventually alter the rocking curve and its time structure.

The authors thank W. Graeff (DESY, Hamburg) and V. Holy (Charles University, Prague) for critical comments on the manuscript.

References

Ackermann, W. *et al.* (2007). *Nat. Photon.* **1**, 336–342.
Ayvazyan, V. *et al.* (2002). *Eur. Phys. J. D*, **20**, 149–156.
Ayvazyan, V. *et al.* (2006). *Eur. Phys. J. D*, **37**, 297–303.
Born, M. & Wolf, E. (1999). *Principles of Optics: Electromagnetic Theory of Propagation, Interference and Diffraction of Light.* Cambridge University Press.
Chapman, H. *et al.* (2006). *Nat. Phys.* **2**, 839–843.
Chukhovskii, F. N. & Förster, E. (1995). *Acta Cryst.* A**51**, 668–672.
DESY Report (2006*a*). *The European X-ray Free-Electron Laser.* DESY, Hamburg, Germany.
DESY Report (2006*b*). *SASE FEL at the TESLA Facility Phase 2.* DESY, Hamburg, Germany.
Eilbeck, J. C. (1972). *J. Phys.* **5**, 1355.
Fechtchenko, R. M., Vinogradov, A. V. & Voronov, D. L. (2002). *Opt. Commun.* **210**, 179–186.
Gerth, Ch., Faatz, B., Lokajczyk, T., Treusch, R. & Feldhaus, J. (2001). *Nucl. Instrum. Methods A*, **475**, 481–486.
Graeff, W. (2004). *J. Synchrotron Rad.* **11**, 261–265.
Hau-Riege, S. P. *et al.* (2007). *Phys. Rev. Lett.* **98**, 145502.
Kogelnick, H. (1969). *Bell Syst. Tech. J.* **48**, 2909–2947.
Kohn, V. G. (1995). *Phys. Status Solidi B*, **187**, 61–70.
Krenza, A. & Meyer-ter-Vehn, J. (2005). *Eur. Phys. J. D*, **36**, 199–202.
Levashov, V. E. & Vinogradov, A. V. (1993). *Appl. Opt.* **32**, 1130–1135.
Lindenberg, A. M. *et al.* (2005). *Science*, **308**, 392–395.
Parratt, L. G. (1954). *Phys. Rev.* **95**, 359–369.
Shastri, S. D., Zambianchi, P. & Mills, D. M. (2001). *J. Synchrotron Rad.* **8**, 1131–1135.
Stojanovic, N. *et al.* (2006). *Appl. Phys. Lett*, **89**, 241909.
Takenaka, H., Ichimaru, S., Nagai, K., Ohchi, T., Ito, H. & Gullikson, E. M. (2005). *Surf. Interface Anal.* **37**, 181–184.
Tatchyn, R. & Bionta, R. (2001). *Proc. SPIE*, **4143**, 89–97.
Vinogradov, A. V., Brytov, I., Grudskii, A., Kogan, M. T. & Kozhevnikov, I. V. (1989). *X-ray Mirror Optics.* Leningrad: Mashinostroenie. (In Russian.)
Wark, J. S. & He, H. (1994). *Laser Part. Beams*, **12**, 507–513.
Wark, J. S. & Lee, R. W. (1999). *J. Appl. Cryst.* **32**, 692–703.